THE JOURNAL OF BIOLOGICAL CHEMISTRY VOL. 284, NO. 8, pp. 5381–5394, February 20, 2009

Tiam1 and Rac1 Are Required for Platelet-activating Factor-induced Endothelial Junctional Disassembly and Increase in Vascular Permeability*

Received for publication, November 26, 2008 Published, JBC Papers in Press, December 17, 2008, DOI 10.1074/jbc.M808958200

Ivana I. Knezevic[‡], Sanda A. Predescu[‡], Radu F. Neamu[§1], Matvey S. Gorovoy[§1], Nebojsa M. Knezevic[§2], Cordus Easington[‡], Asrar B. Malik[§], and Dan N. Predescu[‡3]

From the [‡]Department of Pharmacology, Rush University Medical Center, Chicago, Illinois 60612 and the [§]Department of Pharmacology, College of Medicine, University of Illinois, Chicago, Illinois 60612

It is known that platelet-activating factor (PAF) induces severe endothelial barrier leakiness, but the signaling mechanisms remain unclear. Here, using a wide range of biochemical and morphological approaches applied in both mouse models and cultured endothelial cells, we addressed the mechanisms of PAF-induced disruption of interendothelial junctions (IEJs) and of increased endothelial permeability. The formation of interendothelial gaps filled with filopodia and lamellipodia is the cellular event responsible for the disruption of endothelial barrier. We observed that PAF ligation of its receptor induced the activation of the Rho GTPase Rac1. Following PAF exposure, both Rac1 and its guanine nucleotide exchange factor Tiam1 were found associated with a membrane fraction from which they co-immunoprecipitated with PAF receptor. In the same time frame with Tiam1-Rac1 translocation, the junctional proteins ZO-1 and VE-cadherin were relocated from the IEJs, and formation of numerous interendothelial gaps was recorded. Notably, the response was independent of myosin light chain phosphorylation and thus distinct from other mediators, such as histamine and thrombin. The changes in actin status are driven by the PAF-induced localized actin polymerization as a consequence of Rac1 translocation and activation. Tiam1 was required for the activation of Rac1, actin polymerization, relocation of junctional associated proteins, and disruption of IEJs. Thus, PAF-induced IEJ disruption and increased endothelial permeability requires the activation of a Tiam1-Rac1 signaling module, suggesting a novel therapeutic target against increased vascular permeability associated with inflammatory diseases.

The endothelial barrier is made up of endothelial cells (ECs)[4] connected to each other by interendothelial junctions (IEJs) consisting of protein complexes organized as tight junctions (TJs) and adherens junctions (AJs). In addition, the focal adhesion complex located at the basal plasma membrane enables firm contact of ECs with the underlying basement membrane and also contributes to the barrier function (1–3). The glycocalyx, the endothelial monolayer, and the basement membrane all together constitute the vascular barrier.

The structural integrity of the ECs along with their proper functionality are the two most important factors controlling the tightness of the endothelial barrier. Changes affecting these factors cause loss of barrier restrictiveness and leakiness. Therefore, defining and understanding the cellular and molecular mechanisms controlling these processes is of paramount importance. Increased width of IEJs in response to permeability-increasing mediators (4) regulates the magnitude of transendothelial exchange of fluid and solutes. Disruption of IEJs and the resultant barrier leakiness contribute to the genesis of diverse pathological conditions, such as inflammation (5), metastasis (6, 7), and uncontrolled angiogenesis (8, 9).

Accumulated evidence demonstrated that IEJs changes are responsible for increased or decreased vascular permeability, and the generally accepted mechanism responsible for them was the myosin light chain (MLC)-mediated contraction of ECs (5, 10). However, published evidence showed that an increase in vascular permeability could be obtained without a direct involvement of any contractile mechanism (11–16).

The main component of the vascular barrier, the ECs, has more than 10% of their total protein represented by actin (17), which under physiological salt concentrations subsists as monomers (G-actin) and assembled into filaments (F-actin). A large number of actin-interacting proteins may modulate the assembly, disassembly, and organization of G-actin and of actin filaments within a given cell type. Similar to the complexity of actin-interacting proteins found in other cell types, the ECs

* This work was supported, in whole or in part, by National Institutes of Health Grants RO1-HLO89462 (to S. P.) and PO1-HL60678 (to A. B. M.). This work was also supported by American Heart Association Grant SDG0635175N, and start-up funds from RUMC (to D. N. P.). The costs of publication of this article were defrayed in part by the payment of page charges. This article must therefore be hereby marked "*advertisement*" in accordance with 18 U.S.C. Section 1734 solely to indicate this fact.

[1] Supported by National Institutes of Health Grant RO1-GM 56159 (to Tatiana-Voyno Yasenetskaya).

[2] Supported by National Institutes of Health Grant RO1-HL 84153 (to Dolly Mehta).

[3] To whom correspondence should be addressed: 1735 W. Harrison St., Jelke South Bldg., Rm. 1415A, Chicago, IL 60612. Tel.: 312-563-2436; E-mail: Dan_Predescu@rush.edu.

[4] The abbreviations used are: EC, endothelial cell; AJ, adherens junction; Ab, antibody; EM, electron microscopy; GEF, guanine nucleotide exchange factor; HUVEC, human umbilical vein endothelial cell; IEJ, interendothelial junction; MLC, myosin light chain; NC, nitrocellulose; PAF, platelet-activating factor; PAF-R, platelet activating factor receptor; PDB, peripheral dense band; PLC, phospholipase C; SF, stress fiber(s); TJ, tight junction; siRNA, small interfering RNA; DTT, dithiothreitol; Tricine, *N*-[2-hydroxy-1,1-bis(hydroxymethyl)ethyl]glycine; GST, glutathione *S*-transferase; MOPS, 4-morpholinepropanesulfonic acid.

utilize their actin binding proteins to stabilize the endothelial monolayer in order to efficiently function as a selective barrier (11). In undisturbed ECs, the actin microfilaments are organized as different networks with distinctive functional and morphological characteristics: the peripheral filaments also known as peripheral dense band (PDB), the cytoplasmic fibers identified as stress fibers (SF), and the actin from the membrane cytoskeleton (18). The peripheral web, localized immediately under the membrane, is associated with (i) the luminal plasmalemma (on the apical side), (ii) the IEJ complexes on the lateral surfaces, and (iii) the focal adhesion complexes on the abluminal side (the basal part) of polarized ECs. The SF reside inside the endothelial cytoplasm and are believed to be directly connected with the plasmalemma proper on the luminal as well as on the abluminal side of the cell. As described, the endothelial actin cytoskeleton (specifically the SF) seems to be a stable structure helping the cells to remain flat under flow (19). It is also established that the actin fibers participate in correct localization of different junctional complexes while keeping them in place (20). However, it was suggested that the dynamic equilibrium between F- and G-actin might modulate the tightness of endothelial barrier in response to different challenges (13).

Mediators effective at nanomolar concentrations or less that disrupt the endothelial barrier and increase vascular permeability include C2 toxin of *Clostridium botulinum*, vascular permeability factor, better known as vascular endothelial growth factor, and PAF (21). C2 toxin increases endothelial permeability by ribosylating monomeric G-actin at Arg-177 (22). This results in the impairment of actin polymerization (23), followed by rounding of ECs (16) and the disruption of junctional integrity. Vascular permeability factor was shown to open IEJs by redistribution of junctional proteins (24, 25) and by interfering with the equilibrium of actin pools (26). PAF (1-*O*-alkyl-2-acetyl-sn-glycero-3-phosphocoline), a naturally synthesized phospholipid is active at 10^{-10} M or less (27). PAF is synthesized by and acts on a variety of cell types, including platelets (28), neutrophils (29), monocytes (30), and ECs (31). PAF-mediated activation of ECs induced cell migration (32), angiogenesis (7), and vascular hyperpermeability (33) secondary to disassembly of IEJs (34). The effects of PAF on the endothelium are initiated through a G protein-coupled receptor (PAF-R) localized at the plasmalemma, in a large endosomal compartment inside the cell (34), and also in the nuclear membrane (35). In ECs, PAF-R was shown to signal through $G\alpha_q$ and downstream activation of phospholipase C isozymes (PLCβ_3 and PLCγ_1), and via cSrc (32, 36). Studies have shown that PAF challenge induced endothelial actin cytoskeletal rearrangement (37) and marked vascular leakiness (38); however, the signaling pathways have not been elucidated.

Therefore, in the present study, we carried out a systematic analysis of PAF-induced morphological and biochemical changes of endothelial barrier *in vivo* and in cultured ECs. We found that the opening of endothelial barrier and the increased vascular leakiness induced by PAF are the result of a shift in actin pools without involvement of EC contraction, followed by a redistribution of tight junctional associated protein ZO-1 and adherens junctional protein VE-cadherin.

MATERIALS AND METHODS

General Reagents

The reagents were obtained as follows. PAF and PAF antagonist (BN-52021) were from BIOMOL Research Laboratories; Monastral Blue, phenylmethylsulfonyl fluoride, bovine serum albumin (BSA), Triton X-100, SDS, human thrombin, sphingosine 1-phosphate, and all chemicals for electrophoresis were from Sigma. All EM reagents were from EM Science. Protein A/G immunobeads were from Calbiochem; kits for protein determination and the ECL kits were from Pierce. All GTPase activation kits were from Upstate. Glutathione-Sepharose 4B media/GSTrap 4B columns were from Amersham Biosciences. The plasmid encoding the Rac1 mutant (G15ARac1) was provided by Dr. K Burridge, amplified, and used as described in Ref. 39. The following primary Abs were used: anti-actin (Sigma), anti-PLCβ_3, anti-PLCγ_1, anti-Vav1, anti-phospho-PLCβ_3 and anti-phospho-PLCγ_1 (Cell Signaling Technology); anti-cSrc, anti-phospho-cSrc, and anti-Vav3 (Upstate); mouse monoclonal anti-MLC, anti-phospho-(Ser-18/19) MLC (Abcam), anti-human PAF-R (Cayman Chemical), anti-Rac1, anti-Tiam1, and anti-β-PIX (Santa Cruz Biotechnology, Inc., Santa Cruz, CA); anti ZO-1, anti VE-cadherin, and anti-Vav2 (Zymed Laboratories Inc., San Francisco); anti-Sos1 (BD Transduction Laboratories).

Cell Culture and siRNA Transfections

Cell Culture—HUVECs (Science Cell Technologies) were grown with endothelial growing medium-2 from Cambrex plus 20% fetal calf serum and used between passages 3 and 5. For PAF challenge or for treatments with other reagents, the monolayers were starved of growth factors by changing them in endothelial growth medium-2 plus 0.2% fetal calf serum for 4 h.

siRNA Methodology—For Tiam1 silencing, we used Dharmacon SMART pool reagents and controls. Dharmacon siRNAs duplexes were used as in Ref. 3. We carried out preliminary experiments to establish the optimal conditions (concentration, specific sequence, and time, using the SMART pool) for transfection of cell cultures. HUVECs were transfected at 80–90% confluence with the individual siRNA oligonucleotides, and after the initial screening, the individual Targetplus Smartpool (NM_003253; 5′-PUUCUUUACAGCUUCGGUUCUU-3′) sequence (3 μg) was delivered to >80% confluent monolayers of HUVECs using Dharmafect1 transfection reagent according to the manufacturer's instructions. For control siRNA, a scrambled oligonucleotide template (5′-PCUCAUCUGUCUGUGUCUAUCC-3′) containing the same number of bases as the Tiam1 siRNA target that did not Blast to any gene in the human genome was used. We also used the siCONTROL™ functional nontargeting siRNA sequence 5′-UAGCGACUAAACACAUCAA-3′ as a control for potential secondary effects and the siGloCyclophylin B siRNA for efficiency of transfection and also to evaluate any off-target effects caused by the Tiam1 RNAi in ECs.

Cell Lysates and Cell Fractionation—HUVECs were solubilized in 50 mM Tris-HCl, pH 7.4, 1 mM EGTA, 0.5% SDS, protease inhibitors (1 h at room temperature), and the lysates were clarified by centrifugation (30 min, 40,000 rpm, 4 °C). For ana-

lyzing phosphorylated proteins, the cells were solubilized in a buffer containing 50 mM Tris-HCl, pH 7.5, 1 mM EDTA, 1 mM EGTA, 2 mM sodium orthovanadate, 50 mM sodium fluoride, 1% Triton X-100, 2% SDS, and protease inhibitors. Protein concentration was determined as in Ref. 40. A total membrane fraction was obtained as in Ref. 41 from monolayers of ECs.

In Vivo Administration of PAF

PAF effects on mouse lung microvessels were studied as in Ref. 34. Briefly, 0.1 ml of 5% Monastral Blue was injected in a tail vein, and after 10 min, variable amounts of PAF (0.1–100 ng, final volume of 0.1 ml) were infused into another tail vein. After 15 min, the lungs were fixed and prepared for transmission electron microscopy as in Ref. 34. Thin sections were examined with a JEOL-1220 transmission electron microscope.

Measurement of Actin Filament Assembly

Extraction of G- and F-actin from ECs monolayers was done as in Ref. 42. Briefly, control and PAF-activated ECs were washed with cold PBS, lifted, and centrifuged at 2,000 rpm (5 min, 4 °C); the pellet was resuspended in lysis buffer I (20 mM HEPES-NaOH, pH 7.2, 100 mM NaCl, 1 mM sodium vanadate, 50 mM NaF, 1% Triton X-100, protease inhibitors), for 1 h at room temperature. The lysate was centrifuged at 10,000 rpm (25 min, 4 °C), and the supernates containing G-actin were saved. The pellets were solubilized (1 h, 4 °C) using lysis buffer II (15 mM HEPES-NaOH, pH 7.5, 150 mM NaCl, 1% Triton X-100, 1% sodium deoxycholate, 0.1% SDS, 10 mM EDTA, 1 mM dithiothreitol (DTT), 1 mM sodium vanadate, protease inhibitors) and centrifuged at 45,000 rpm, and the supernates containing F-actin were further used.

MLC Phosphorylation

Control and PAF-stimulated ECs were washed with cold PBS and treated with a cold solution of 10% trichloroacetic acid, 2 mM EDTA, 10 mM DTT as in Ref. 43. The cells were collected and centrifuged (5 min, 4 °C) in a Beckman Microfuge; the pellet was washed three times with cold acetone containing 2 mM DTT and solubilized in SDS sample buffer without bromphenol blue and DTT. After measuring the protein content, bromphenol blue, SDS, and DTT were added, and the extract was subject to electrophoresis using NUPAGE gels (4–12% bis-Tricine) according to the manufacturer's instructions, transferred to nitrocellulose (NC) membranes, incubated with specific Abs, and developed as described below.

Immunoblotting and Immunoprecipitation

Imunoblotting—For immunoblotting, 80 μg of protein/lane were run at 150 V, and the transfer was done as in Ref. 44. Strips of NC were incubated with the primary Abs and processed as in Ref. 41. The reaction was visualized using the ECL kit and HyBlot CL Autoradiography Film.

Phosphorylation—The phosphorylation of different proteins was assessed using NC membranes blocked (1 h, room temperature) with a buffer containing 1% nonfat dry milk, 1% BSA, 0.05% Tween 20, 2 mM sodium orthovanadate, 50 mM sodium fluoride, and 2 mM sodium pyrophosphate, which were incubated with the phospho-specific Abs, washed, and developed as above. The NC membranes were striped (30 min, 50 °C in 1 M Tris-HCl, pH 6.8, 10% SDS, 10 mM β-mercaptoethanol), reprobed with Abs against the nonphosphorylated proteins, and developed.

Immunoprecipitation—For immunoprecipitation, 1 mg/ml total protein of precleared cell lysates (incubation with 50 μl of Protein A/G slurry, 2 h, room temperature, centrifuged at 14,000 rpm) and the supernates were incubated with the primary Ab (2 h, room temperature). The antigen-antibody (Ag·Ab) complexes were recovered by incubation with 20 μl of Protein A/G slurry overnight, followed by centrifugation (10 min, 14,000 rpm, 4 °C). From washed beads, Ag·Ab complexes were solubilized in sample buffer and resolved on a 4–20% SDS-PAGE minigel.

Immunofluorescence

Confluent monolayers of HUVECs were washed with ice-cold PBS, fixed/permeabilized with methanol (5 min, −20 °C), blocked with 1% BSA in PBS (PBS-BSA) for 1 h at room temperature, and incubated with the following primary Abs: anti-Tiam1, anti-ZO-1, and anti VE-cadherin, for 1 h at room temperature, washed with 0.1% BSA in PBS, incubated with the corresponding secondary Abs diluted in PBS-BSA (1 h, room temperature), washed again, mounted with Prolong-antifade mounting medium, and examined with a Carl Zeiss Axioplan 2 fluorescence microscope. Phalloidin-fluorescein isothiocyanate (Molecular Probes) staining for actin was performed as in Ref. 45.

Rho GTPase Activation Assays

The GTPase activity of Rac1, Cdc42, and RhoA was measured as in Refs. 35 and 36. Cells were rinsed with cold PBS and lysed in radioimmune precipitation buffer (50 mM Tris-HCl, pH 7.4, 150 mM NaCl, 1% Triton X-100, 0.25% deoxycholate, 1.5 mM $MgCl_2$, 1 mM EGTA, 1 mM phenylmethylsulfonyl fluoride, 10 mM NaF, 10 mM pervanadate). The lysates were clarified by centrifugation (16,000 × *g* for 10 min). After protein determination, equal amounts of total protein (400 – 600 μg) were incubated with 50 μg of GST fusion proteins for 30 min at 4 °C. The activities of RhoA and Cdc42 were measured as per the manufacturer's protocols and as described in Ref. 46. The p21 PDB of PAK expressed as a GST fusion protein was used to precipitate GTP-bound Rac1 from controls and PAF-treated cell lysates. The precipitated Rac1 was subjected to SDS-PAGE followed by immunoblotting, and the amount of active Rac1 was measured as in Ref. 47 by densitometric analysis using ImageJ software (National Institutes of Health).

Precipitation of Activated GEFs with Recombinant Rac1 Protein

The pull-down assay with nucleotide-free Rac1 mutant (G15ARac1), was performed as in Ref. 48. PAF-treated and -untreated monolayers were lysed in a buffer containing 1% Triton X-100, 20 mM HEPES, pH 7.4, 150 mM NaCl, 5 mM $MgCl_2$, and protease inhibitors, clarified by centrifugation (16,000 × *g* for 10 min), and equal amounts of protein (~500 μg) were incubated for 60 min at 4 °C with 30 mg of GST or GST fusion proteins containing nucleotide-free Rac1 protein (G15ARac1)

bound to glutathione-Sepharose. The beads were washed four times with lysis buffer, separated in a minigel, and transferred to NC membranes. The membranes were first stained with Poanceau S to assure that similar amounts of fusion proteins were used in all experiments and then immunoblotted with Abs against Vav1–3, β-PIX, Sos1, and Tiam1.

Scanning EM

For scanning EM, HUVECs were grown on polylysine-coated glass coverslips and prepared as in Ref. 49. The monolayers were rinsed with PBS, fixed with 2.5% glutaraldehyde in PHEM buffer (15 min, room temperature), submerged in 1% tannic acid in 0.1 M cacodylate buffer, pH 7.2, overnight, postfixed in 1% OsO_4 in 0.3 M sodium cacodylate for 15 min, washed with water for 5 min, dehydrated through increasing concentrations of ethanol, and exchanged to pure hexamethyldisilazane. The monolayers were coated with a 4-nm layer of a platinum-carbon mixture using a Cressington sputter coater, observed at 15–20 kV and micrographed using a Jeol SM 6320F field emission scanning EM. Fixation and processing of selected tissue specimens for transmission electron microscopy was as in Ref. 41.

Statistical Analysis

Data were compared using one-way analysis of variance, Student's *t* test with a Bonferoni correction for multiple comparisons, and a two-way analysis of variance where needed. Statistical significance was set at $p < 0.05$.

RESULTS

PAF Induces Severe Endothelial Barrier Disruption—The effects of *in vivo* administration of PAF were investigated on the mouse lung vascular bed, after its intravenous administration. First, we injected intravenously Monastral Blue, an electron opaque tracer with 0.5–3-μm molecular dimensions and after 5 min PAF as described under "Materials and Methods." Morphological analysis at the EM level, following challenge with 100 nM PAF for 15 min, demonstrated focal openings of IEJs in postcapillary venules (Fig. 1*A*), capillaries (Fig. 1*B*), and muscular venules (data not shown) that allowed the free passage of not only Monastral Blue (*arrows* in Fig. 1, *A* and *B*) but also blood cells (note in Fig. 1*A*, an opened IEJ "plugged" by a platelet). These focal openings were associated with intramural deposits made up of the tracer, platelets, and even erythrocytes escaping from circulation but retained by the basement membrane (Fig. 1, *A* and *B*). The edges of ECs at the level of gaps showed characteristic finger-like projections with lengths of 1–5 μm and thickness of 0.1–0.3 μm that were tightly packed and belonged to one or the other contiguous EC (Fig. 1*B*, F_1 and F_2). These membrane projections, mainly filopodia, cramming the IEJs and extending from one cell to another were one of the most evident effects of PAF on interendothelial spaces morphology *in vivo*. We also detected fenestrae subtended by diaphragms in capillary (Fig. 1*C*, *arrows*) and venular lung endothelia (Fig. 1*D*), which are normally of the continuous type, as well as the presence of large vacuoles 0.4–3 μm in diameter (Fig. 1, *A* and *B*).

The results of an extensive morphometric analysis shown in Table 1 document the extent of PAF-induced alterations in the murine lung vascular bed. We observed (i) that 30% of capillary IEJs and 45% of postcapillary venule IEJs were open, (ii) a large number of fenestrations, up to 5 units/1 μm of cellular length, (iii) a thickening of the basement membrane from 0.3 to 0.5 μm in capillaries and from 0.35 to 0.53 μm in the venular end of the murine lung vascular bed, and (iv) the formation of a considerable number of large vacuoles (10–14 times greater after PAF challenge than under basal conditions).

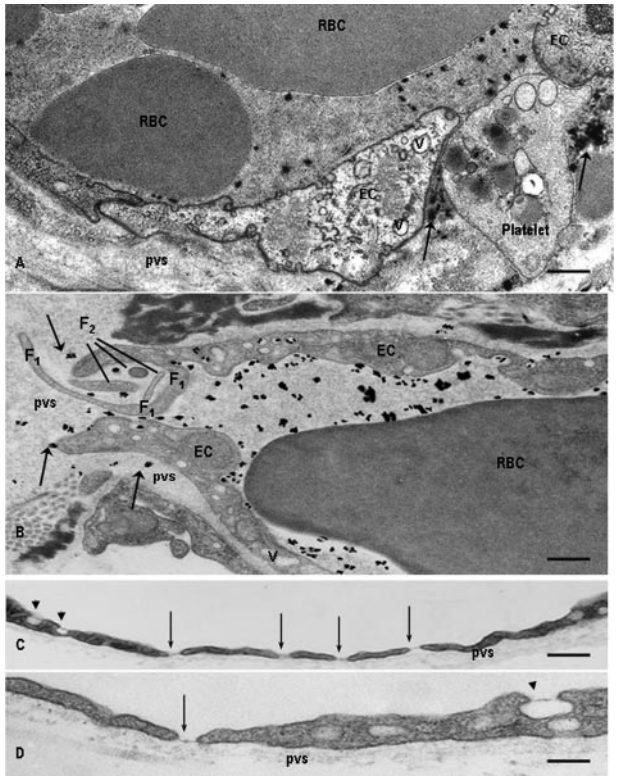

FIGURE 1. **Morphological alterations induced by PAF in mouse lung microvessels.** *A*, opening of large gaps (~1 μm) in the endothelium of a lung venule. Platelet and Monastral Blue particles (*arrows*) have escaped through the interendothelial gap and are retained in the perivascular space (*pvs*) by the basement membrane. Note the presence of red blood cells (*RBC*) and Monastral Blue tracer within the vascular lumina. *Bar*, 350 nm. *B*, interendothelial gaps encountered in the lung capillaries. A gap of ~2 μm was crammed with fingerlike projections (F_1 and F_2) in the endothelium of a capillary. Note the escaped particles of Monastral blue (*arrows*) and the presence of long cellular extensions belonging to one cell (F_1) as well as the existence of sectioned intercellular projections (F_2) that could belong to any of the two ECs facing the gap. In both *A* and *B*, the ECs facing the open gaps have a higher than normal number of intracellular vacuoles (*v*). *Bar*, 250 nm. *C* and *D*, typical fenestrae (*arrows*) found in venular (*C*) or capillary (*D*) endothelium. After PAF administration, classic fenestrations closed by diaphragms were found both in the capillary and venular end of the murine lung vascular bed. There is a tendency for PAF-induced fenestrae to be grouped in the venular endothelium (*C*). Also note that some of the luminally opened vesicles (*arrowheads*) in *C* and *D* are provided with a diaphragm. *Bar*, 175 nm; the micrographs are representative of five experiments.

A system of cultured ECs was used to unravel the cellular determinants responsible for the above mentioned PAF effects. Confluent monolayers of ECs (3 days postconfluence) were used for a time course analysis of PAF effects on IEJs. PAF (10^{-10} M) was applied for different time periods from 1 to 30 min. We detected opened IEJs as early as 1 min that, over time, increased in number and surface (Fig. 2*A*, compare *b*–*e* with *a*). The extent of IEJ opening analyzed by morphometry is summarized in Table 2. The number of gaps was >7 times increased at

TABLE 1

Morphometric analysis of structural changes induced by *in vivo* administered PAF in the murine lung vascular bed

The vascular segments were identified, on micrographs at ×42,500 final magnification, based on their luminal diameters, 30 mm for arteries, between 10 and 20 mm for arterioles, <9 mm for capillaries, between 10 and 30 mm for venules, and 40 mm for veins. n = number of micrographs on which the vascular segment was identified. *, $p < 0.001$; ‡, $p < 0.01$. BM, basement membrane.

Vascular segment	Aggregated area		Open junctions		Fenestrations		BM thickness		Large vesicles (>200 nm)	
	Control	PAF	Control	PAF	Control	PAF	Control	PAF	Control	PAF
	μm^2		% of total		No./μm length		μm			
Artery (n = 98)	47 ± 5	55 ± 8	0	0	0	0	0.32 ± 0.05	0.34 ± 0.08	0	0
Arteriole (n = 122)	86 ± 1	79 ± 4	0	<0.5	0	1.5 ± 0.3*	0.33 ± 0.07	0.32 ± 0.09	0	11 ± 2
Capillary (n = 388)	568 ± 29	487 ± 39	0	33 ± 7*	0	5.4 ± 0.6*	0.29 ± 0.07	0.51 ± 0.06‡	18 ± 3	227 ± 11
Venule (n = 294)	371 ± 15	406 ± 22	18 ± 2	49 ± 6*	0	6.2 ± 0.3*	0.39 ± 0.08	0.58 ± 0.07‡	37 ± 8	542 ± 31
Veins (n = 228)	209 ± 11	271 ± 31	17 ± 3	32 ± 5*	0	2.8 ± 0.9*	0.37 ± 0.05	0.53 ± 0.05‡	49 ± 1	288 ± 29

15 min and >10 times by 30 min post-PAF compared with control (undisturbed) ECs.

When monolayers of ECs, activated by PAF, were stained with phalloidin-fluorescein isothiocyanate to investigate the distribution of actin, we noted (i) the development of large lamelipodia (Fig. 2*A*, *b*, *thick arrows*) and (ii) a shift in the distribution of intracellular actin from a characteristic well defined PDB and some central SF scattered inside the cell (Fig. 2*A*, *a*) to mainly SF in the first minutes after PAF (Fig. 2*A*, *b* and *c*). Both the SF and the PDB were markedly diminished beyond 15 min (Fig. 2*A*, *d* and *e*). The actin redistribution induced by PAF administration was reversed within 60 min after washing PAF (data not shown) and was PAF-R-dependent as long as it was inhibited by pretreatment of confluent HUVEC monolayers with BN-52021 (50) a PAF-R antagonist (Fig. 2*A*, *f*).

PAF-induced interendothelial openings contained two types of extensions: finger-like projections extending between two ECs (Fig. 2*A*, *c–e*) along with larger membrane protrusions that were shorter and more polymorphous belonging usually to one EC (Fig. 2*A*, *arrows* in *b*). In addition, within 15 min of PAF exposure, EC shape changed drastically, with cells beginning to elongate (Fig. 2*A*, *d* and *e*). These alterations in actin were not observed when the inactive analog lyso-PAF (50 μM) was used (data not shown) and also were PAF-R-dependent, since the PAF-R antagonist BN-52021 prevented them (data not shown).

The dramatic PAF-induced changes, seen by light microscopy, imply the presence of PAF-R scattered all over the endothelium that are transducing signals responsible for the pleiotropic structural changes reported.

High Resolution Scanning EM Analysis of PAF-induced Morphological Alterations—Confluent monolayers of ECs were employed to better define the structural changes recorded at light microscopy. Besides recording open IEJs, with wide gaps present between opposing cells (Fig. 2*B*, compare *b–d* with *a*) as soon as 1 min after PAF challenge; we also detected many filopodia (Fig. 2*B*, *b–d*) and lamellipodia (Fig. 2*B*, *b*) between contiguous ECs with lengths ranging from 1 to 5 μm and diameters from 0.1 to 0.3 μm. Filopodia number increased with time (Fig. 2*B*, *e* and *f*, *versus a–c*), and they were present not only at the level of newly formed gaps but also on the rest of endothelial surface (Fig. 2*B*, *c*, *arrowheads*). At this level of resolution, however, we did not found evidence of endothelial contraction (Fig. 2*B*, *b–d*). The wrinkles seen in some cells, especially in the first 5 min after PAF (Fig. 2*B*, *b*, *arrow*), represent membrane folds covering the newly formed SF inside ECs.

PAF Signals a Reversible Shift of G- to F-actin—To analyze the effects of PAF on actin status, we separated G- and F-actin from both control ECs and cells subjected to PAF treatment, as described under "Materials and Methods." Densitometric analysis of isolated actin pools indicated that (i) under normal conditions, 57% of cell actin is found as F-actin and 43% as G-actin, as shown in Fig. 2*C*, *control*; (ii) within 1 min after PAF, F-actin content increased significantly (68%) and remained elevated for 5 min (77%); (iii) by 15 min, the equilibrium between G- and F-actin was shifted toward G-actin, such that monomeric actin was increased by 30%, with a maximum of 45% at 30 min over the control. The shift of actin was not seen with lyso-PAF (50 μM) applied for 30 min (Fig. 2*C*). Also, pretreatment of EC monolayers with BN-52021 (60 min before PAF) prevented the alterations in cellular actin (Fig. 2*D*).

PAF-R Engagement Changes the Position of TJ-associated and AJ Components—Since PAF-induced IEJ disruption could be the result of displacement of junctional complexes, we addressed this possibility by examining the morphological and biochemical subcellular distribution of TJ-associated ZO-1 protein and AJ protein VE-cadherin. The fluorescent morphological surveys document that the quasicontinuous beltlike pattern of ZO-1 staining in unstimulated monolayers (Fig. 3*A*, *control*) is altered and could be seen as an interrupted signal at the cell periphery at early time points (Fig. 3*A*, 1 min and 5 min) and as a diminished staining (Fig. 3*A*, 15 min) after 15 min of PAF treatment. A similar response was evident for VE-cadherin that was redistributed only from the areas where the ECs were no longer in direct contact (Fig. 3*B*, *arrows* in 1 min–5 min). VE-cadherin staining was seen as short breaks on its distribution, at the cell periphery, but still present, even if less intense, at the level of remaining cell-cell contacts (Fig. 3*B*, 1 min and 5 min, *arrowheads*). The intracellular staining for ZO-1 was invariably more marked than for VE-cadherin. Because the PAF-induced changes in the staining for the two proteins is very suggestive of their redistribution inside EC, we further characterized quantitatively their redistribution by Western blot and densitometric analysis. Although the amounts of ZO-1 and VE-cadherin, in total cell lysates, did not reveal any differences between PAF-treated and control monolayers (*lower panels* in Fig. 3, *B* and *D*, respectively), when their distribution was assessed in the membrane fractions of endothelial monolayers, we found a rapid redistribution for both IEJ proteins. As shown in the *upper panels* of Fig. 3, *B* and *D*, we noticed a more pronounced redistribution for ZO-1 than for VE-cadherin. The accompanying

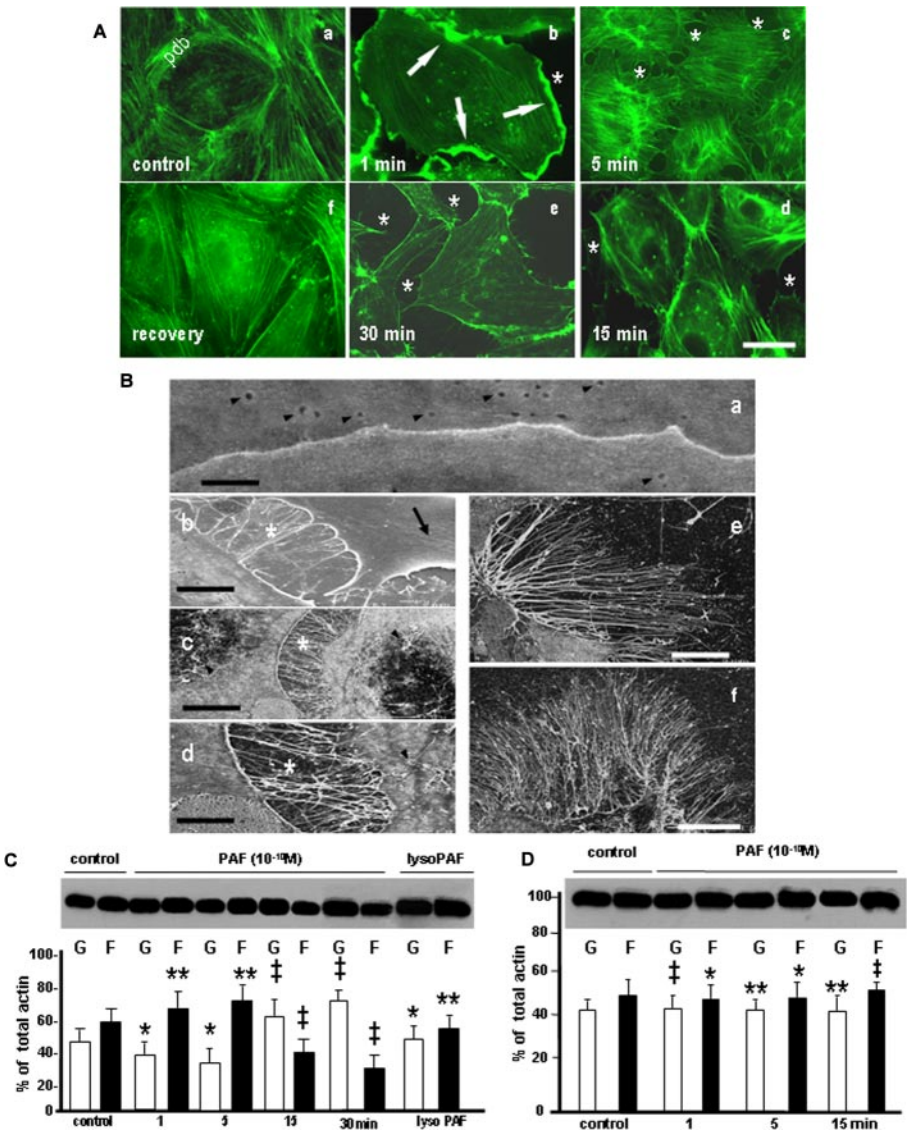

FIGURE 2. **PAF-induced structural and biochemical alterations of endothelial actin pools.** *A*, phalloidin staining of endothelial actin in control conditions and after PAF-R activation. Actin staining of growth hormone-starved monolayers (*control*) showed the presence of a well organized peripheral dense band (*PDB*) and the existence of a few stress fibers (*SF*) scattered in the center of the cell. When confluent monolayers of HUVECs were stimulated with PAF for 1 min, 5 min, 15 min, and 30 min (*e*), we observed the formation of large cellular folds in the first 1 min (*b*, *arrows*), the dilation of IEJs (*asterisk* in *b–e*), the dissolution of PDB (*c–e*), and the formation of SF in the first 5 min (*b* and *c*). These alterations were less numerous at the later time points (*d* and *e*). The mentioned changes of endothelial cell shape and of endothelial actin pools are PAF-R-dependent, since the treatment of the monolayer with BN 52078 prevented them (*e*). *Bar*, 30 μm in *a*, *b*, *e*, and *f* and 25 μm in *c* and *d* ($n = 8$). *B*, high resolution field emission scanning EM of PAF-induced alterations in endothelial cells. *a*, the IEJ between two resting ECs appears as a *continuous line* without interruptions or irregularities. The figure also illustrates the presence of plasmalemmal openings of endothelial vesicular carriers on both cells (*arrowheads*). *Bar*, 0.1 μm ($n = 6$). *b*, IEJ gaps formed between endothelial cells that are filled with filopodia and lamellipodia (*asterisk*). The wrinkles present on the surface of one of the endothelial cells (*arrow*) represent plasma membrane folds over the newly formed SF inside the cell. *Bar*, 1 μm ($n = 6$). *c*, within 5 min of PAF exposure, there is a marked increase in membrane projections (especially filopodia), and the newly formed filopodia are also found on the surface of PAF-treated cells (*arrowheads*). *Bar*, 5 μm ($n = 6$). *d*, by 15 min after PAF exposure, membrane projections remained abundant, whereas the dimensions (width and length) of IEJs gaps increased. *Bar*, 2 μm ($n = 6$). *e* and *f*, the number and length of the filopodia were maximal by 30 min. *Bar*, 5 μm for *e* and 10 μm for *f* ($n = 6$ in both cases). *C* and *D*, PAF-R activation induced the shift of G- to F-actin. *C*, different pools of actin from confluent monolayers of HUVECs were analyzed by immunoblotting with an anti-actin polyclonal Ab. The *panel* illustrates changes in G- and F-actin pools in control and PAF-treated (10^{-10} M) monolayers. Note the changes in G- and F-actin from basal conditions (*control*) to more F-actin in the first 5 min and the reversal of the ratio (with much more G-actin) at 15 and 30 min. The *last lanes* show that lyso-PAF (10^{-6} M for 30 min) did not change the ratio of different pools of actin ($n = 8$). *D*, the blot shown illustrates the absence of actin pool changes induced by PAF challenge following pretreatment of monolayers with the PAF-R antagonist BN 52078 ($n = 6$). Statistical significance was as follows: *, $p < 0.01$; **, $p < 0.05$; ‡, $p < 0.001$, by comparison with controls (Student's *t* test).

graphs confirm that there is a reduction of ~40% of ZO-1 *versus* a reduction of only ~20% in VE-cadherin in the membrane.

The PAF-induced morphological alterations (lamelipodia, filopodia, SF) backed up by biochemical changes in actin status, along with the formation of interendothelial gaps are usually interpreted as resulting from the contraction of endothelial cytoskeleton in a process mediated by MLC phosphorylation. To gain more details about the molecular mechanisms triggered by PAF challenge, we decided to investigate the phosphorylation status of MLC.

PAF Disrupts IEJs in the Absence of MLC Phosphorylation—We next examined MLC phosphorylation using an Ab recognizing only the phosphorylated Ser^{18}/Thr^{19} from MLC (Fig. 4) to address whether PAF-induced endothelial junction disruption is MLC phosphorylation-dependent. PAF concentrations from 10^{-12} to 10^{-6} M failed to induce phosphorylation of MLC, whereas thrombin (the positive control) induced a robust phosphorylation (Fig. 4, *lane f*). Using a NUPAGE system that allows a clear separation of different MLC isoforms, the signal obtained with phosphorylation-specific Ab after PAF (Fig. 4, *lanes b–e*) was not different from the signal obtained in unstimulated ECs (Fig. 4, *lane a*), and it was in contrast to the prominent changes observed after thrombin on all four isoforms (Fig. 4, *lane f*). The finding that MLC is not phosphorylated after PAF prompted us to look for other downstream effectors involved in PAF-R signaling, responsible for interendothelial gap formation. With this intent, we studied the phosphorylation of enzymes known to influence the status of actin (cSrc and PLC) in other cells (51–53).

PAF Induces cSrc, PLCβ_3, and PLCγ_1 Activation Downstream of PAF-R—Confluent, growth factor-starved endothelial monolayers were stimulated with PAF, and

phosphorylation of cSrc, PLCβ, and PLCγ was assessed using specific anti-phospho-Abs. As shown in Fig. 5, *A*, *B*, and *C* (*middle*), each enzyme was phosphorylated in a time-dependent manner. cSrc was phosphorylated within 1 min after PAF, remained active for 15 min (Fig. 5*A*, *middle*), and then was dephosphorylated by 30 min. Of different isoforms of PLCβ and PLCγ examined, we observed that only PLCβ_3 (Fig. 5*B*, *middle*) and PLCγ_1 (Fig. 5*C*, *middle*), were phosphorylated after PAF. PAF induced an immediate phosphorylation of PLCβ_3, reaching a maximum between 15 and 30 min and returning to basal level after 60 min (data not shown). PLCγ_1 was also phosphorylated within 1 min and returned to basal level by 30 min. Phosphorylation in each case was PAF-R-dependent, since the receptor antagonist BN-52021 blocked the response (Fig. 5, *A–C*, *top panels*). The total amounts of enzymes did not change during the experiment (Fig. 5, *A–C*, *bottom panels*).

TABLE 2

The number of gaps induced in confluent HUVEC monolayers under different experimental conditions

The values reported represent the number of gaps between neighboring ECs counted on 200 mm^2 of monolayer surface. 5–9 different slides were used for every experimental condition. The results are means ± S.D.

Experimental conditions	0 min	1 min	5 min	15 min	30 min
Undisturbed	25 ± 2	25 ± 4	24 ± 3	23 ± 4	26 ± 5
PAF-treated	25 ± 3	52 ± 6	144 ± 15	198 ± 19	312 ± 21
BN-52021 + PAF	23 ± 4	26 ± 5	25 ± 3	24 ± 4	26 ± 2
siRNA Tiam1	26 ± 5	29 ± 4	28 ± 7	32 ± 6	31 ± 3
siRNA Tiam1 + PAF	26 ± 2	41 ± 4	81 ± 7	87 ± 6	92 ± 5

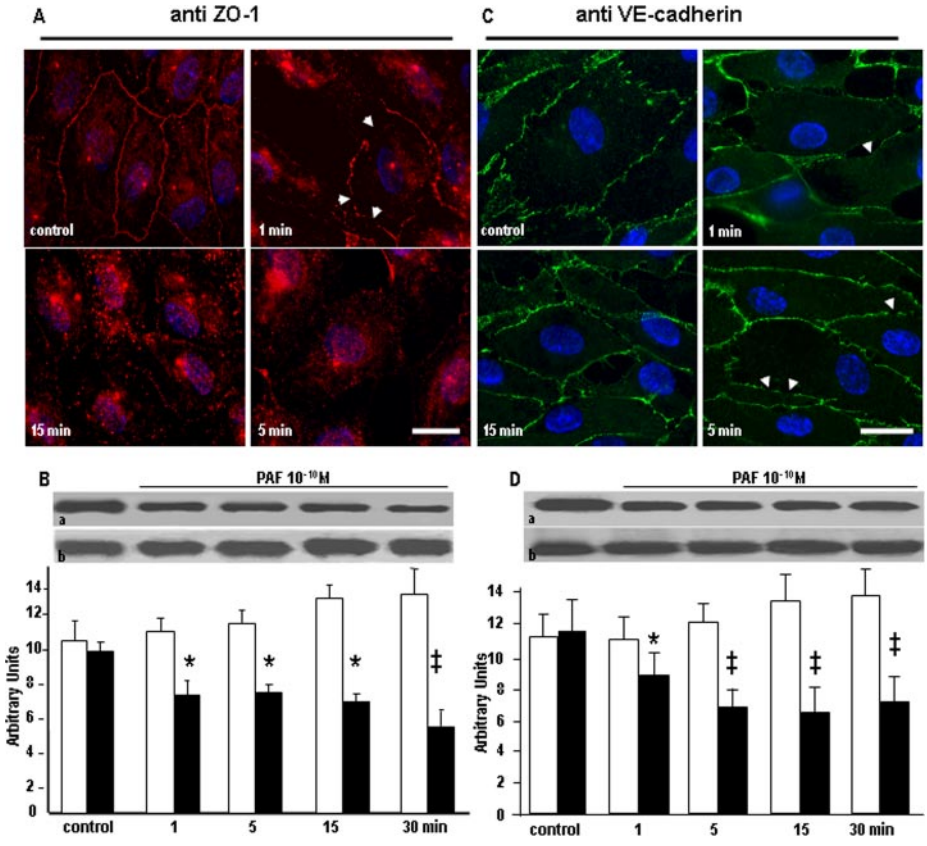

FIGURE 3. **Redistribution of ZO-1 and VE-cadherin after PAF-R activation.** *A*, immunofluorescence staining of ZO-1. In unstimulated HUVECs (*control*), the signal for ZO-1 is distributed in a prominent beltlike structure underlining the cell circumference with a less intense and more diffuse pattern inside the cell. At 1 min after PAF, the beltlike pattern is preserved, but discontinuities begin to appear, with the stain disappearing in some areas (*top right*, *arrowheads*). After 5 min, the staining is seen as discontinuous puncta at the level of IEJs, and a much stronger signal is present inside the cell and within the nucleus (*bottom left*). By 15 min, the signal at the level of IEJs is reduced to very few puncta, whereas the scattered signal from the cytoplasm is much more diffuse (*bottom right*) ($n = 5$). *Bar*, 24 μm. *B*, ZO-1 shift from membrane. Western blot analysis of VE-cadherin presence in the membrane fraction (*a*) and in the total cell lysate (*b*) shows its redistribution after PAF challenge. The accompanying *graph* documents the >30% decrease of VE-cadherin in the isolated endothelial membranes ($n = 6$). Statistical significance was as follows: *, $p < 0.01$; ‡, $p < 0.001$ *versus* control (paired Student's *t* test). *C*, VE-cadherin signal after PAF challenge. In resting HUVECs, the VE-cadherin staining shows the characteristic "chicken wire" pattern at the level of interendothelial boundaries indicative of its presence at the level of AJs (*control*). In cells treated with PAF for 1 and 5 min, the staining is apparent only at IEJs where the cells are still in contact (*arrows* in *top right* and *bottom left*). However, within 15 min, the staining of the membranes facing the newly formed interendothelial gaps was greatly diminished (*bottom right*), and its distribution around the periphery of the cell was patchy ($n = 4$). *Bar*, 25 μm. *D*, VE-cadherin redistribution in PAF-stimulated cells. The Western blots of VE-cadherin from membranes (*a*) and total cell lysate (*b*) strongly suggest that after PAF challenge, there is a redistribution of the protein between the two lysates, and the associated *graph* documents the >20% timely changes induced by PAF. Statistical significance was as follows: *, $p < 0.01$; ‡, $p < 0.001$ by contrast with controls (Student's *t* test).

PAF-R Ligation Signals to Rac1—Since PAF-R activation caused membrane protrusions shown in Fig. 2 as a result of changes in the endothelial actin status, we surmised that PAF-R signaling induced activation of Rho GTPases, Rac1, RhoA, or Cdc42, known to mediate formation of lamellipodia and filopodia. We observed that PAF-R stimulation, in the first 15 min after PAF, increased Rac1-GTP levels (Fig. 6*A*), which started to decrease after 30 min. However, RhoA (Fig. 6*B*) and Cdc42 (Fig. 6*C*) were not activated by PAF in the time frame used in our study. Still, RhoA was activated by thrombin (10 units/ml) treatment for 15 min (54) or by sphingosine 1-phosphate (5 μM) challenge (55), as shown in Fig. 6*B*. Different from RhoA, the treatment of HUVECs with thrombin also induced Cdc42 activation but only after 1 h of treatment (Fig. 6*C*), whereas sphingosine 1-phosphate did not change the amounts of Cdc42-GTP at any time point studied (data not shown). Unlike the relatively unchanged RhoA and Cdc42 activation response, PAF-induced Rac1 activation was robust and prolonged. These results clearly indicate that PAF-R engagement induces selectively the activation of Rac1 without concomitant activation of RhoA and Cdc42.

PAF challenge of EC monolayers also induced Rac1 translocation from cytosol to the membrane fraction within 1 min (Fig. 7*A*, *a*). Rac1 remained associated with the membrane fraction for up to 15 min, whereas its total amount did not change (Fig. 7*A*, *a versus b*). As shown in the accompanying *graph*, there was an increase of membrane-associated Rac1 from <20% in con-

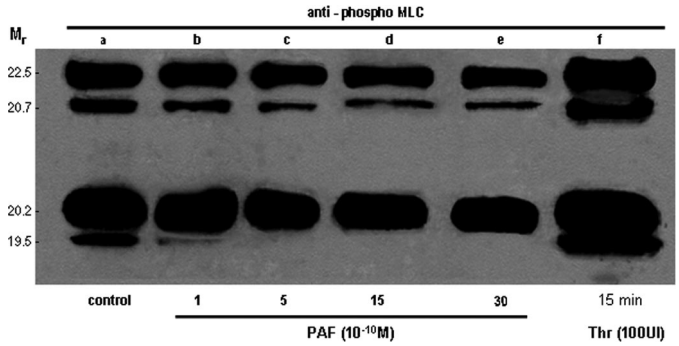

FIGURE 4. **PAF fails to induce phosphorylation of myosin light chain in endothelial cells.** Western blot of transferred NUPAGE electrophoretogram (4–12% polyacrylamide and MOPS as a running buffer) of total EC lysates, probed with anti-phospho-tMLC Abs, showing the resolved isoforms of MLC. As illustrated in *lane a*, there is a basal phosphorylation of endothelial MLC in growth hormone-starved and unstimulated HUVECs. *Lanes b–f* demonstrate the phosphorylated isoforms of MLC when phosphospecific polyclonal Ab was used for detection. *Lanes b–e* show that there is no phosphorylation in any of the MLC isoforms after PAF exposure for 1 min (*b*), 5 min (*c*), 15 min (*d*), or 30 min (*e*). *Lane f* demonstrates that thrombin (100 IU, for 15 min) induces a robust phosphorylation of all four isoforms of MLC. The gel is representative for five experiments.

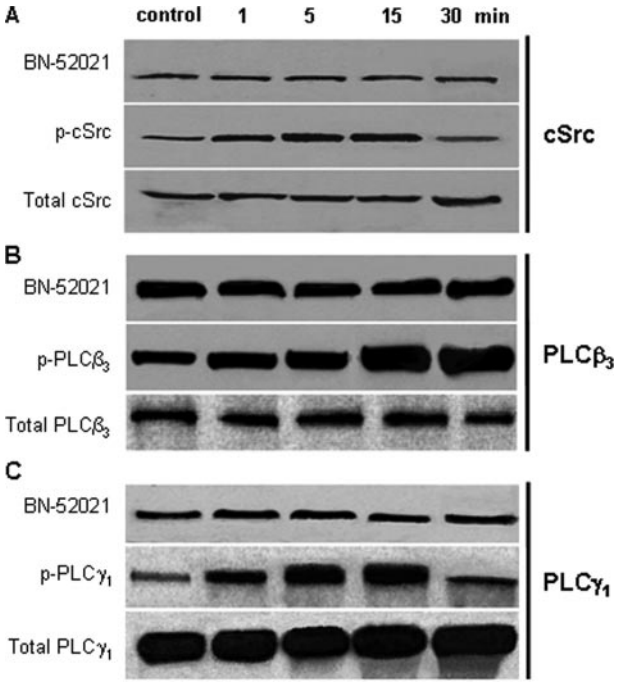

FIGURE 5. **Phosphorylation of cSrc and PLCβ_3 and PLCγ_1 isoforms of PLC induced by PAF.** *A*, activation of cSrc by PAF began as early as 1 min, extends beyond 15 min, and returns to nearly basal level by 30 min (*middle*). The *lower panel* shows that the total amount of cSrc is relatively low in HUVECs and did not change after PAF-R ligation. The *upper panel* shows that its activation is PAF-R-dependent, since pretreating the monolayers with BN 52021 (30 min, room temperature, 1 μM) prevented the response ($n = 4$). *B*, phosphorylation of PLCβ_3 was detected after 1 min of PAF exposure and was much stronger by 15 min as shown in the *middle panel*. The *lower panel* illustrates that the total amount of PLCβ_3 present in HUVECs did not change, whereas the *upper panel* proves that the activation of the enzyme was prevented by BN 52021 pretreatment ($n = 4$). *C*, phosphorylation of PLCγ_1 was evident at 1 min after PAF; it was greater after 5 min, continued for the following 10 min, and returned to basal levels by 30 min as illustrated in the *middle panel*. The *lower panel* shows that the total amount of PLCγ_1 did not change, whereas the *upper panel* demonstrates that pretreating the monolayers with BN 52021 prevented the response ($n = 4$).

trols to >40% by 5 and 15 min. Based on these data, and keeping in mind that our testing included only the most studied small GTPase (RhoA, Cdc42, and Rac1), we can surmise that the robust activation of only Rac1 after its translocation to the EC membranes is the signature of PAF-induced activation of ECs. Since Rac1 is activated and translocated to the membrane after PAF challenge, we next investigated the exchange factor involved.

The GDP/GTP Exchange Factor Tiam1 Mediates PAF-induced Rac1 Activation—First we investigated which Rac1 GEFs are expressed in ECs. We identified in control monolayers of HUVECs a rich presence of Vav2, β-PIX, Sos-1, Tiam1, and in much smaller amounts the presence of Vav3 by immunoblotting (Fig. 7*B*). Then, to determine which GEF might be involved in Rac1 activation downstream of PAF-R ligation, we used nucleotide-free Rac1 mutant G15ARac1 in a pull-down strategy based on its higher affinity for binding active GEFs than the native Rac1. We found that PAF treatment increased the association of Tiam1 with G15ARac1 (Fig. 7*C*, *BEADS*). Control experiments using GST showed no evidence of nonspecific GFP binding (data not shown). The same mutant failed to pull down Sos1 and Vav3, suggesting that they are not involved in PAF signaling in ECs. Low levels of β-PIX and even lower levels of Vav2 were detected binding to the G15ARac1 mutant, but their binding was not increased by PAF treatment. These results clearly indicate that, of the GEFs examined, only the association of Tiam1 with G15ARac1 is increased after PAF binding to its receptor.

Morphological surveys of Tiam1 redistribution, after PAF challenge of confluent and growth factor-starved HUVECS, confirmed its translocation to the endothelial plasma membranes. Our light microscopy data illustrate that in growth hormone-starved ECs, the signal for Tiam1 was scattered throughout the cytosol without preferential association with any subcellular compartment (Fig. 7*D*, *a*, *control*). However, within 1 min of PAF exposure, Tiam1 staining at the plasmalemma became prominent (Fig. 7*D*, *b*), with staining still being detected by 5 min (Fig. 7*D*, *c*). Membrane-associated Tiam1 staining (even if less intense than in the first minute) was also detected by 15 min (Fig. 7*D*, *d*).

Biochemical evidence obtained by Western blotting of a membrane fraction proved that only Tiam1 was translocated to a membrane fraction, after PAF treatment (Fig. 7*E*, *top*), whereas total Tiam1 amount did not change (Fig. 7*E*, *bottom*). Moreover, the quantitative analysis of Tiam1 translocation (associated *graph*) indicated that 20% of total Tiam1 is transferred to the membrane after 15 min of PAF treatment, whereas under control conditions, <5% of total Tiam1 is associated with the membrane fraction. In the same time frame, its total amount remained unchanged (Fig. 7*E*). Note also that when Tiam1 was down-regulated (Fig. 7*E*), even if we loaded 150 μg of total protein per lane, we did not detect its presence in the membrane.

Tiam1 Is Required for Rac1 Activation after PAF-R Activation—The requirement for Tiam1 in mediating Rac1 activation after PAF-R ligation was demonstrated by down-regulating Tiam1 protein expression with specific siRNA. As shown, the specific siRNA sequence used was able to reduce the protein amount by >80% at 96 h after transfection (Fig.

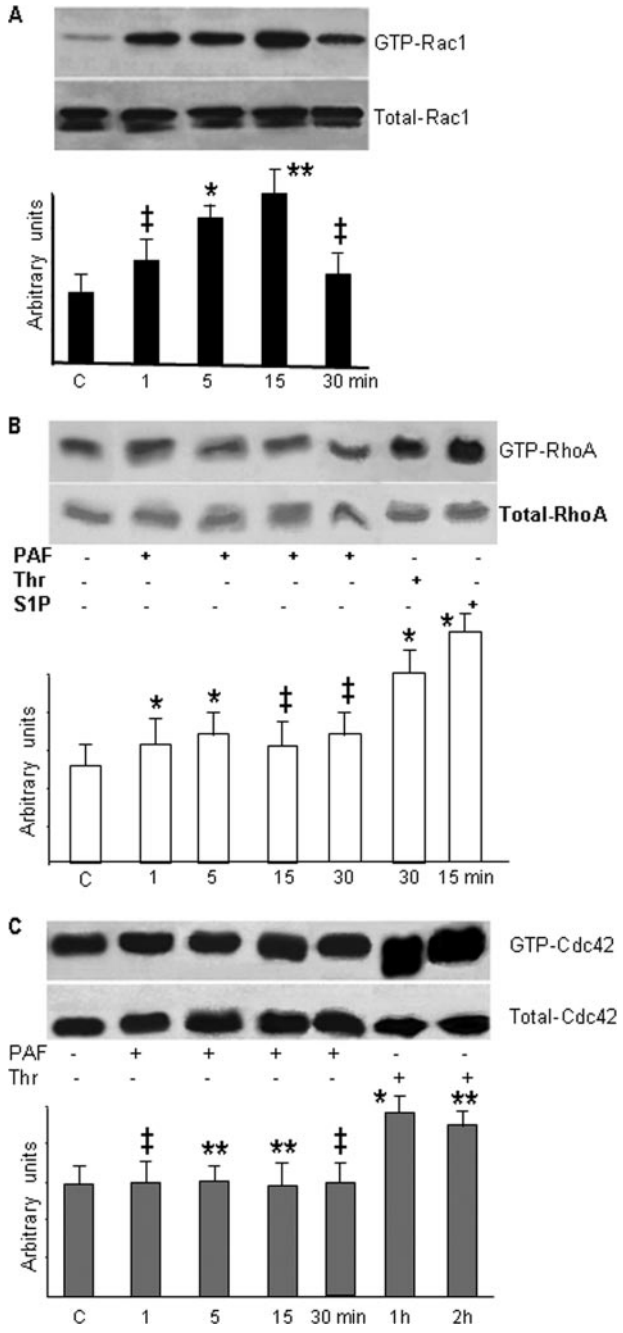

FIGURE 6. **PAF selectively activates Rho GTPase Rac1.** *A*, Rac1 is the only small GTPase activated. Western blot shown in the *upper panel* demonstrates the activation of Rac1 after PAF treatment, whereas the *lower panel* shows that the total amount of Rac1 is not modified ($n = 10$). Note that Rac1 activation returns to basal level by 30 min. Quantitative measurements are shown in the associated *bar graph*. *B*, RhoA was not activated, as shown by the Western blot from the *upper panel*. The *lower panel* illustrates that the total amount of RhoA present in the monolayers did not change. Summary data from different experiments are presented in the *bar graph* ($n = 5$). Note the changes in the status of RhoA after thrombin (10 IU, 30 min), its bigger activation after sphingosine 1-phosphate (5 μM, 15 min), and its unchanged status after PAF. *C*, Cdc42 was also not activated at any time point after PAF challenge ($n = 5$), and the total levels remained relatively unchanged, as shown in the *lower panel*. The summary *bar graph* represents studies in confluent monolayers. Statistical significance for *A–C* is as follows: *, $p < 0.01$; **, $p < 0.05$; ‡, $p < 0.001$ (paired Student's *t* test).

8*A*, *a*), whereas the scrambled siRNA used as control did not affect Tiam1 levels at all time points studied (Fig. 8*A*, *b*). In the same time frame (0–96 h after siRNA transfection), the levels of other two Rac1 GEFs (β-PIX and Vav2) were unaffected (Fig. 8*A*, *c* and *d*). These results signify that the siRNA used is specific for Tiam1 and prompted us to perform all experiments at this time point.

Tiam1 Down-regulation Prevents Rac1 Activation, Its Membrane Translocation, and Interendothelial Gap Formation—Tiam1 down-regulation prevented Rac1 activation, as determined by the pull-down assay (Fig. 8*B*). The quantitative analysis shows that there are no differences in the amount of GTP-Rac1 brought down after PAF challenge.

Tiam1 down-regulation also impaired Rac1 translocation to the membrane fraction (Fig. 8*D*). We did not find any change in the amounts of Rac1 (Fig. 8*D*, *graph*) associated with the isolated membranes after PAF in EC monolayers treated with siRNA.

We also observed that down-regulation of Tiam1 reduced the number of gaps formed in the monolayer after PAF exposure (Fig. 8*E*). To substantiate the role of Tiam1 in mediating IEJ gap formation, we assessed by morphometric analysis the effects of Tiam1 down-regulation on PAF-induced gaps. The results presented in Table 2 document (i) the dramatic increase in IEJ gaps induced by PAF (5-fold) *versus* undisturbed monolayers and (ii) a greater than 45% decrease in the number of gaps induced by PAF treatment of Tiam1-depleted *versus* ECs with normal Tiam1 levels. We found an average of 25 IEJ gaps/200 mm^2 on control monolayers, *versus* 146 IEJ gaps/200 mm^2 of EC monolayer surface in cells subjected to PAF challenge and only 66 IEJ gaps/200 mm^2 of monolayer surface in ECs deficient in Tiam1 after PAF challenge.

The morphological alterations recorded after Tiam1 down-regulation (reduction in the number of IEJ gaps) were matched at the biochemical level by an impeded shift from G- to F-actin (Fig. 8*F*) after PAF. The associated *graph* documents that the ratio of G- to F-actin of 44–56% in the control monolayers changes to a ratio of 49–51% in the PAF-challenged monolayers at any time studied.

Association of Tiam1 and Rac1 with PAF-R after PAF Exposure—We next addressed, by immunoprecipitation, the relationship between PAF-R and the membrane-translocated Tiam1 and Rac1 before and after PAF exposure. Of the Rac1 GEFs studied (Tiam1, Vav2, β-PIX, and Sos-1), Tiam1 was the only GEF studied that co-immunoprecipitated with the PAF-R (Fig. 9).

Total cell lysates prepared from control and PAF-treated cells were incubated with a specific anti-PAF-R Ab, and when the immunoprecipitates were probed with anti-Tiam1 and anti-Rac1 Abs (Fig. 9*A*), both proteins were found to be associated with PAF-R only after PAF challenge. Tiam1 and Rac1 were not associated with PAF-R under basal conditions (Fig. 9*A*, *control*), but the association occurred as rapidly as 1 min after PAF stimulation (Fig. 9*A*). When the same lysates were immunoprecipitated with anti-Tiam1 Ab and the immunoprecipitates were probed with anti-PAF-R and anti-Rac1 Ab, we found the same interaction, no association under basal conditions (Fig. 9*B*, *control*), and a rapid (1-min) association after PAF exposure that lasted as long as 15 min (Fig. 9*B*, PAF (10^{-10} M)).

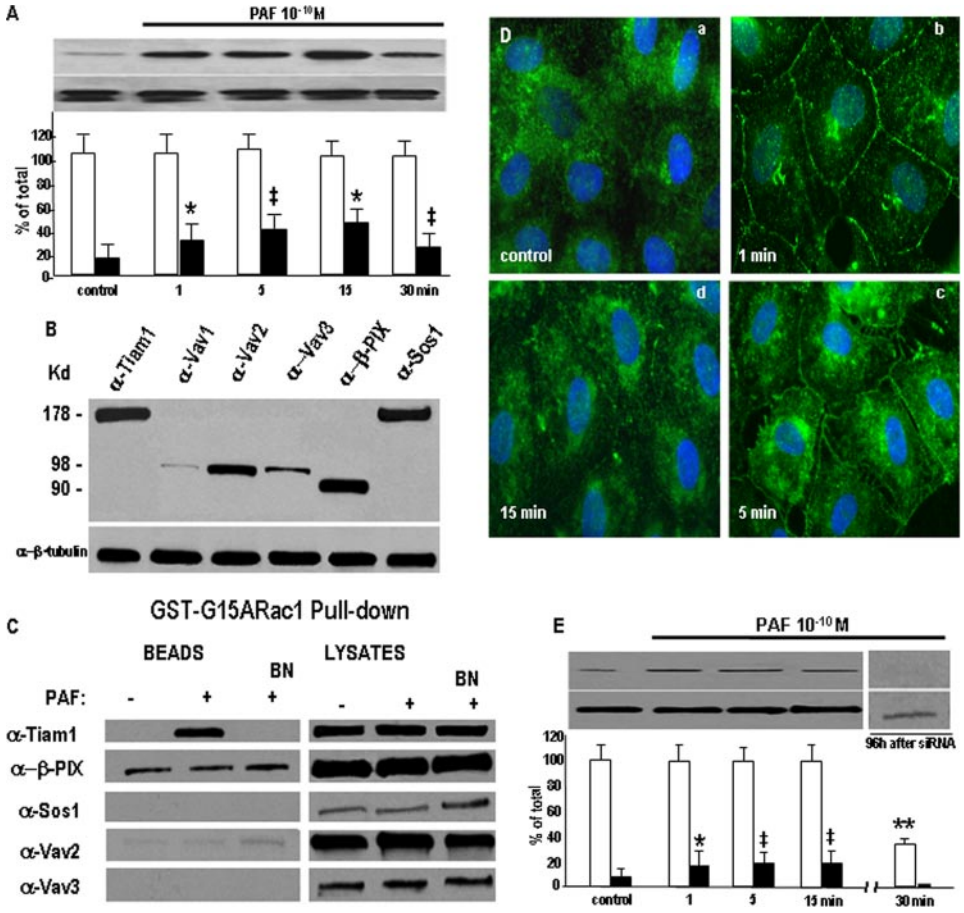

FIGURE 7. **Tiam1 is the Rac1 GEF activated and membrane-translocated after PAF-R engagement.** *A*, translocation of Rac1 to the membranes. The *upper panel* of the Western blot illustrates that Rac1 is translocated to a total membrane fraction in the first 15 min and returns to near basal levels by 30 min after PAF challenge, whereas the *lower panel* demonstrates the abundance of Rac1 in HUVECs as detected upon Western blotting of total cell lysates probed with an anti-Rac1 Ab ($n = 4$). Integrated results from all experiments are presented in the associated *graph* that documents the ~2.5-fold increase of the membrane-associated Rac1 (*black columns*) in the first 15 min after PAF treatment and the marginal modification of total Rac1 (*white bars*). Statistical significance is as follows: *, $p < 0.01$; ‡, $p < 0.001$ by contrast with controls (Student's *t* test). *B*, Tiam1 is present in HUVEC. The Western blot from *upper panel* illustrates the presence of different GEFs for Rac1 in the total cell lysates of HUVECs. From the GEFs studied, Tiam1, Sos1, and β-PIX are well represented, whereas from the three Vavs, only Vav2 is found in large amounts. The blot shown in the *lower panel* was obtained from a total cell lysate immunostained first with the above Abs, striped, and then probed with an anti-β-tubulin Ab to show equal loading of total protein ($n = 8$). *C*, GST pull-down assay for detection of the GEF activated by PAF. The GST-G15ARac1 beads and the lysates used for pull-down were probed with the same Abs as in *B* in conditions when PAF was present (+) or absent (−) or in the presence of PAF-R inhibitor BN-52021 (*BN*), and as illustrated, only Tiam1 was brought down from PAF-treated lysates, whereas the treatment of monolayers with the specific inhibitor BN blocked the interaction of Tiam1 and PAF-R. The signal obtained with β-PIX, on the beads, is nonspecific as long as is not modified by either PAF or BN treatment. *D*, morphological assessment of Tiam1 redistribution. Staining of hormone-starved HUVECs with anti-Tiam1 Abs shows its scattered distribution all over the cell under basal conditions (*control*, *a*), the changes in its distribution within 1 min (*b*) after PAF with the signal becoming prominent at the level of IEJs, and the presence of the staining still associated with IEJs at 5 min (*c*) and also by 15 min (*d*). Note that the anti-Tiam1 staining was detected in newly formed membrane projections ($n = 6$). *Bar*, 20 μm. *E*, Tiam1 translocation to the membrane. The presence and the behavior of Tiam1 in a total membrane fraction was questioned by Western blotting analysis, and as shown in the *upper panel* there is an increase in the amount of Tiam1 associated with the membrane induced by PAF treatment, whereas its total amount does not change (*lower panel*). The accompanying *graph* shows that there is an increase of more than 4-fold, from <5% in control to >25% by 15 min, of membrane-associated Tiam1 ($n = 8$). Statistical significance was as follows: *, $p < 0.01$; ‡, $p < 0.001$ (paired Student's *t* test). The interrupted *blot* and the associated *graph* show that at 96 h after Tiam1 down-regulation, there is no PAF-induced association of Tiam1 with the membrane fraction ($n = 9$). Statistical significance was as follows: **, $p < 0.05$.

To gain a better insight on the role played by Tiam1 on the formation of this supramolecular complex, EC monolayers were treated with siRNA for Tiam1 and then with 10^{-10} M PAF. A total membrane fraction was isolated and immunoprecipitated as above. The results of co-immunoprecipitation of the membrane fraction demonstrate no association between PAF-R with Tiam1 and Rac1 when anti-PAF-R Ab was used (Fig. 9*C*) and the same when the anti-Tiam1 Ab was utilized (Fig. 9*D*). PAF treatment did not induce the association of Rac1 with PAF-R in the absence of Tiam1. The lack of association between PAF-R and Rac1 in cells depleted in Tiam1 and their independence of PAF treatment (compare controls *versus* time points) strongly supports the idea of a supramolecular complex formed on the membrane-localized PAF-R after PAF challenge.

DISCUSSION

The selective barrier of the vessel wall formed mainly by the continuous monolayer of endothelium depends structurally and functionally on the integrity of its cytoskeleton. Early on, it was rationalized that a functional endothelial barrier is the result of the equilibrium between an intermediate contractile status of ECs (determined by the status of actin and myosin) and tightly organized IEJs (both TJ and AJ) (5, 56, 57). As a consequence, it is still thought that the activation of EC contraction is the main (if not the only) mechanism behind the formation of interendothelial gaps induced either experimentally or pathologically (2, 58), and this is true for most of the biologically active substances tested but not for all. It was also established that there are biologically active substances that do not activate EC contraction, and some of them (PAF, vascular endothelial growth factor, and C2 toxin of *C. botulinum*) are recognized as being the most potent in inducing the formation of interendothelial gaps. Therefore, it is logical for us to advance the idea that there are at least two classes of substances capable of disturbing the endothelial barrier: the most potent ones (active between 10^{-9} and 10^{-12} M) that are modifiers of the endothelial actin and a much larger class of compounds that are less potent (active over 10^{-7} M) that act by inducing actomyosin interaction and generating contractile responses. In order to better define and to start to unravel the cellular and molecular mechanisms transducing the effects of the compounds belonging to the first class, we decided

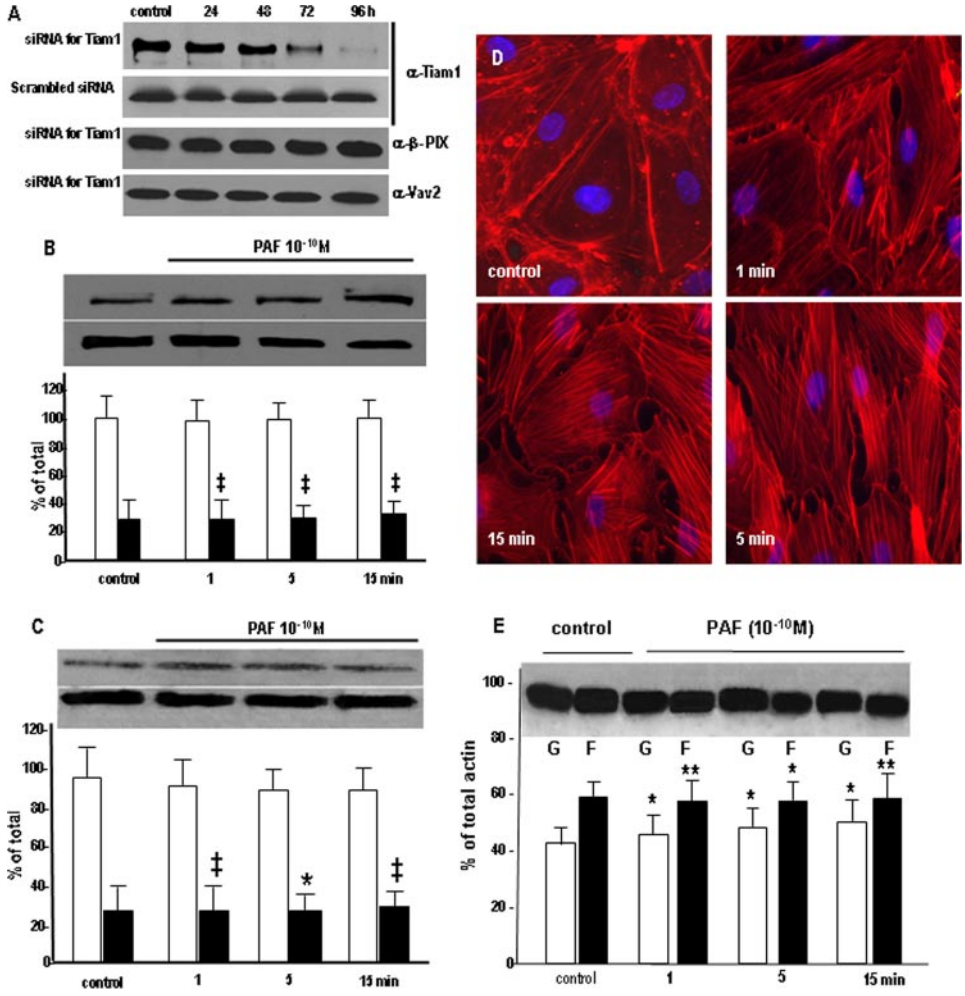

FIGURE 8. **Effects of Tiam1 down-regulation on PAF-induced signaling.** *A*, Tiam1 down-regulation. HUVECs treated with siRNA specific for Tiam1 showed a gradual decrease in the total amount of protein starting at 48 h, with a >80% reduction seen at 96 h, as demonstrated by Western blotting of EC lysate probed with anti-Tiam1 Ab. Note that the scrambled sequence of the specific siRNA did not change the levels of Tiam1 at any time point. The specific siRNA sequence did not affect the expression of β-Pix and Vav2 Rac1 GEFs, as shown in the *bottom two panels* ($n = 6$). *B*, Tiam1 down-regulation effects on Rac1 redistribution. The *top panels* shows that there is no modification in the amount of Rac1 in the membrane fraction (*upper panel*) as well as in its total amount (*lower panel*), whereas the associated *graph* quantitatively substantiates the lack of Rac1 redistribution at 96 h after Tim1 knockdown; compare with Fig. 7*A* ($n = 7$). Statistical significance was as follows: ‡, $p < 0.001$ (paired Student's *t* test). *C*, Rac1 activation is affected by Tiam1. The activation of Rac1 as detected by the pull-down assay is drastically impaired when Tiam1 is down-regulated and the monolayers are stimulated with PAF, as illustrated in the *upper panel*. However, the total amount of Rac1 is not affected under the same conditions as shown in the *lower panel* ($n = 6$). Statistical significance was as follows: *, $p < 0.01$; ‡, $p < 0.001$ (paired Student's *t* test). *D*, Tiam1 knockdown effect on interendothelial gaps. When the distribution of endothelial actin assessed by staining with fluorescein isothiocyanate-phalloidin was investigated after Tiam1 down-regulation, we did not found it, under basal conditions, changed (compare with the *control panel* from Fig. 2*A*, *a*). *b–d* show the distribution of cellular actin in monolayers of HUVEC after Tiam1 depletion and exposure to PAF for different periods of time ($n = 4$). Under these conditions, there is a redistribution of actin toward a polymerized status; however, note the dramatic reduction in the number of inter endothelial gaps, filopodia, and lamellipodia (compare with Fig. 2, *a–e*) ($n = 8$). *Bar*, 22 μm. *E*, Tiam1 affects the actin shift. The Western blot shows inhibition of actin shift after Tiam1 down-regulation. Challenging the Tiam1-depeleted monolayers with PAF prevented the G- to F-actin shift (compare with Fig. 2*C*) ($n = 4$). Statistical significance was as follows: *, $p < 0.01$; **, $p < 0.05$, by comparison with controls (Student's *t* test).

to study PAF effects on the endothelial monolayer. The mechanism of PAF-induced disruption of endothelial barrier structure and function is incompletely understood, although PAF is recognized to mediate increased vascular permeability (33) and is involved in the pathogenesis of many inflammatory diseases (7). *In vivo* experiments in the cat hind limb (59), human and rat skin (60, 61), rat venules (12), rat and mouse cremaster (33, 34), hamster cheek pouch (62), and sheep lung (63) show that PAF increases markedly vascular permeability to water and macromolecules. Here we show, using *in vivo* studies, that the engagement of PAF-R caused (i) focal openings of IEJs mostly in capillaries and postcapillary venules, (ii) widening of IEJs, (iii) formation of lamellipodia and filopodia in the affected IEJs, (iv) a shift of G- to F-actin, and (v) formation of endothelial fenestrations and large intracytoplasmic vacuoles.

We found in the first 5–10 min after PAF challenge a rapid increase in the SF content of ECs, followed by a reduction to the basal level within 30 min. Since PAF challenge induces a dramatic reorganization of endothelial actin network (lamelipodia, filopodia, and SF), we hypothesized that the classical assembly mechanisms of filopodia and lamellipodia are involved. The Arp2/3-mediated actin polymerization is responsible for the short, branched actin filaments that produce the physical force for protrusion found in lamelipodia (64), whereas the Ena/VASP and the formins are in charge with the formation of long parallel actin filaments arranged into tight bundles found in filopodia (65, 66). The investigation of the detailed steps of lamellipodia and/or filopodia formation is beyond the purpose of this work; however, it is one of the future directions of study in our laboratory, and our unpublished data[5] point toward the involvement of both Arp2/3 and Ena/VASP as factors involved in controlling the status of endothelial actin after PAF challenge.

The SF are prominent subcellular structures found in the first 1 min after PAF stimulation. However, under different circumstances, their assembly was rationalized to be essentially a RhoA-mediated process, and since RhoA is not activated after PAF, we assume that, as in the case of EGF (19, 67), the mDIA-interacting protein (DIP) could be phosphorylated by cSrc. In the case of EGF, the activated DIP phosphorylates Vav2, which induces actin polymerization, whereas in

[5] I. I. Knezevic, S. A. Predescu, R. F. Neamu, M. S. Gorovoy, N. M. Knezevic, C. Easington, A. B. Malik, and D. N. Predescu, unpublished data.

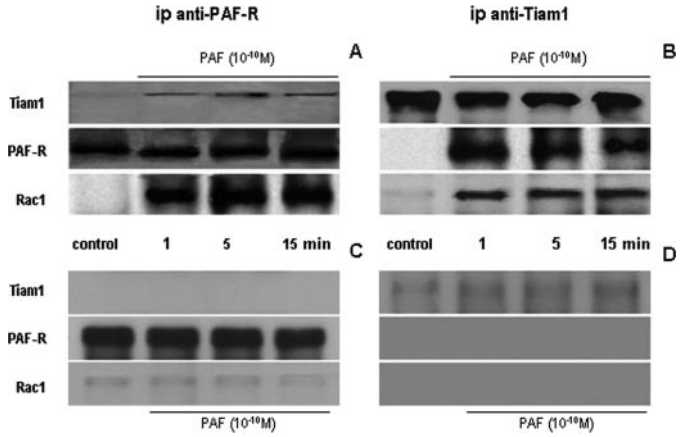

FIGURE 9. **Co-immunoprecipitation of PAF-receptor with Rac1 and Tiam1 is induced by PAF.** *A* and *B*, immunoprecipitation of PAF-R in normal HUVECs. *A*, Western blots of cell lysates prepared from controls and PAF-stimulated monolayers that were immunoprecipitated with anti-PAF-R Ab, showing the immune complexes resolved on SDS-PAGE minigels, transferred to NC membranes, and probed with anti-Tiam1 Ab (*top*), anti-PAF-R (*middle*), and anti-Rac1 Ab (*bottom*). Tiam1 and Rac1 were associated with PAF-R after its ligation, whereas there was no association of the receptor with Rac1 or Tiam1 under basal condition ($n = 6$). *B*, when EC monolayers were immunoprecipitated with anti-Tiam1 Ab and corresponding NC membranes were probed with anti-Tiam1 (*top*), anti-PAF-R Ab (*middle*), and anti-Rac1 Ab, the same association of PAF-R with Rac1 and Tiam1 was found. There was a strong signal for Tiam1, the absence of immunostaining for PAF-R, and the faint staining for Rac1 in controls (*c*) but a strong signal for all proteins within 1 min and all the way up to 15 min after PAF challenge ($n = 6$). *C* and *D*, immunoprecipitation of PAF-R from monolayers depleted in Tiam1. *C*, when the same experiments as in *A* and *B* were repeated with monolayers depleted in Tiam1, we are showing that there is no association between PAF-R and Rac1 in unstimulated cells (*control*) or cells stimulated with PAF. The anti-PAF-R did not bring down any Tiam1, as illustrated in the *upper panel*, but was able to immunoprecipitate the receptor from the HUVECs, as shown in the *middle panel*, and to bring down very low amounts of Rac1, as documented in the *lower panel* ($n = 5$). *D*, the low amounts of Tiam1 precipitated from total lysates, in Tiam1-depleted cells, show that we are down-regulating its expression and not removing all of it from the cell, as shown in the *upper panel*. However, under this condition, we did not detect any signal for the PAF-R (*middle*) or for Rac1 (*bottom*) ($n = 5$).

the case of PAF-R, activated cSrc phosphorylate DIA, which, after activation, binds and phosphorylates a yet unidentified Rac1 GEF to facilitate the activation of Rac1. Moreover, it was demonstrated that cSrc phosphorylation of DIA inhibits Rho activation, whereas SF formation is not affected in NIH3T3 fibroblasts (67); therefore, there are pathways of SF formation that do not depend in the activation of RhoA. The Rac1-dependent but RhoA-independent mechanism of EGF-induced SF formation in fibroblasts needs to be verified in the case of PAF and to be validated in an endothelial background.

All actin changes were evident, at a cellular scale, in the shift of G- to F-actin in the PAF-exposed cells. Since these alterations were prevented by PAF-R antagonist, they are solely ascribed to the effects of PAF-activated signaling.

Changes in the actin-based cytoskeleton were suggested to be involved in the function of the apical junctional complex (TJ and AJ together) either by contraction of the actin ring or by transmission of signals directly to TJ or AJ proteins (68–70). The mentioned work postulated that some types of stimulation of members of the Rho family may result in only modest local changes in actin cytoskeleton and hence only changes in permeability properties of TJ, whereas stimulation of several pathways that converge to activate Rho may cause a major reorganization of the actin cytoskeleton and, hence, the dissociation of the apical junctional complex. Based on our data related to redistribution of ZO-1 and VE-cadherin after PAF-R engagement, we can state that the robust activation of only Rac1 causes a radical reorganization of the actin cytoskeleton, which finally stimulates the dissolution of the apical junctional complex. This is a direct demonstration that the dissociation of interendothelial junctions could be induced by only one small GTPase if its activation is strong enough to induce radical reorganization of actin cytoskeleton in the absence of MLC activation.

We are proving that PAF did not induce MLC phosphorylation in contrast to the well described effects of thrombin and histamine known to increase endothelial permeability by MLC phosphorylation and consequently by an endothelial contraction-dependent mechanism (2, 5, 10). Our results are in agreement with studies showing the absence of MLC involvement in PAF-induced increase in endothelial permeability (12, 71). However, the phosphorylation status of MLC was never proved using biochemical methods. Therefore, our findings, besides substantiating published data, provide new information documenting the fact that inflammatory mediators can increase endothelial permeability by distinctly different mechanisms (*i.e.* those requiring MLC phosphorylation and those that mediate the response by a MLC activation-independent mechanism). PAF, as well as *C. botulinum* C2 toxin, belongs in the latter group, since it relies on signaling events that directly modified IEJs without EC contraction. Therefore, we propose that, besides the classical contraction mechanism, the dynamic of cellular actin is a more sensitive system that controls the tightness of endothelial barrier.

We report that PAF disrupted the integrity of endothelial barrier by localized, Rac1-mediated actin polymerization at the level of cellular membranes. After 15 min of PAF treatment (when the equilibrium of cellular actin is shifted toward G-actin), the endothelial alterations were similar to the effect of C2 toxin of *Clostridium* that also induces a shift toward G-actin (16), even if the initial signaling mechanisms involved are different.

We next investigated PAF-activated signaling pathways responsible for opening of IEJs. We observed a rapid PAF-R-activated phosphorylation of cSrc, PLCβ_3, and PLCγ_1 occurring in the same time frame as IEJ opening. We concluded, based on these data, that PAF-R, besides being a PLC-coupled receptor that utilizes most or some of the down effectors of PLC signaling pathway, utilizes, also, cSrc to induce unique events responsible for its unusual biological potency. Our results are therefore consistent with the reported PAF-induced activation of these enzymes (36, 72); however, it remains to be established which are the individual events responsible for coupling the changes in the activities of these enzymes with the recorded increases in vascular permeability. Since the activation of phosphoinositide-specific PLC is known to induce a rapid hydrolysis of the phosphoinositides present on the cytoplasmic face of the membrane (73) and some of the affected inositol phospholipids are involved in Tiam1 tethering to the plasma membrane (74), it is tempting to speculate that the changes in the status of phosphoinositides from the cytoplasmic face of endothelial membrane, by one of the activated PLC isoforms, generates the

molecular species necessary for Tiam1 translocation and/or activation. After its translocation (which may be facilitated by the PLC-generated phosphoinositides), the phosphorylation of Tiam1 by the mDIA is accomplished by the activated (phosphorylated) cSrc. Another possible mechanism of Tiam1 activation could take place via PLCγ1 that was shown to phosphorylate Tiam1 in NIH3T3 fibroblasts after platelet-derived growth factor (75). Moreover, PAF-stimulated Tiam1 and Rac1 translocation are both PAF-R-dependent and become detectable after 1 min and remain at the same location (membrane) for the next 15 min, suggesting that these findings may be connected.

It is beyond the purpose of this study to investigate the exact mechanisms of Tiam1 translocation, activation (phosphorylation), and tethering with the PAF-R on the membrane, but we provide structural and biochemical data that undoubtedly prove the involvement of the newly formed signalosome (PAF-R + Tiam1 + Rac1) in initiating and controlling the fate of actin pools inside ECs after PAF-R engagement. Nevertheless, it remains to be investigated in detail which are the starting signals that induce the formation of the signaling module based on the membrane-localized PAF-R. Because PAF caused the formation of endothelial membrane lamellipodia and filopodia, we focused on the involvement of Rho GTPases in induced actin shift that cause disruption of IEJs and finally dysfunction of endothelial barrier.

We propose that the hallmark of PAF-R ligation is the translocation and activation of Rac1 without the concomitant activation of RhoA and Cdc42, and we are putting forward the idea that PAF signaling controls Rac1 activity in a time-dependent manner. Currently, it is still unclear how specific exchange factors couple G-coupled receptor signaling to Rho proteins, thereby allowing these proteins to finely coordinate, in time and space, biological responses. Although some studies propose the involvement of Rac1 in endothelial response to PAF (71, 76), the pathways between PAF-R signaling and Rac1-controlled actin status were not explored. In this study, we identified Tiam1 as the GEF responsible for Rac1 activation and found that both Tiam1 and Rac1 associates with PAF-R, after PAF stimulation, resulting in the formation of a PAF-R·Tiam1·Rac1 supramolecular complex. Our results demonstrated that the PAF-induced redistribution of Rac1 and Tiam1 from their intracellular pool to the membrane-localized PAF-R occurs in the same time frame with the F- to G-actin shift. Together, these results indicate that Tiam1 plays a critical role in the response to PAF. Hence, PAF-induced translocation and activation of Tiam to the endothelial membrane associated with the translocation and robust activation of Rac1 may be crucial for its ability to induce Rac1-mediated actin polymerization and consequently most of the plasma membrane ruffle reported in this study (77).

To address the causal relationship between Tiam1 activation and IEJ disruption induced by PAF, we used the siRNA approach to suppress Tiam1 expression. Reduction in Tiam1 expression by >80% prevented the PAF-induced Rac1 activation and localized actin polymerization, resulted in marked diminution in the formation of membrane protrusions at the level of IEJs, and induced a significant (>50%) decrease in the number of interendothelial gaps. Moreover, knockdown of Tiam1 not only inhibited the PAF-induced Rac1 activation but also inhibited PAF-induced actin shift. Thus, we can conclude that (i) Tiam1 mediated the activation of Rac1 in response to PAF challenge, (ii) the exchange factor Tiam1 mediates PAF signaling to Rac1, and (iii) Tiam1 is involved in PAF-induced actin polymerization via activation of Rac1. These results provide strong support for the concept that Tiam1 is the critical signal required for Rac1 activation and localized actin polymerization, which together disrupt IEJs as a consequence of changes in actin status and redistribution of components of TJ and AJ.

Our findings demonstrate (i) the critical role of Tiam1-Rac1 signaling module in mediating the PAF-induced shift in actin followed by IEJ disassembly and (ii) that there could be increased endothelial permeability without MLC-mediated cell contraction.

Acknowledgments—We greatly appreciate the gift of GST-G15ARac1 cDNA from Dr. K. Burridge (University of North Carolina, Chapel Hill, NC) and the technical support in preparing the samples for EM and high resolution scanning electron microscopy of Nicky Watson (Whitehead Institute, Cambridge, MA), Kristina Jarosius, and Linda Juarez (EM Core Facility, University of Illinois, Chicago, IL). This work was started when Dan Predescu worked at the Department of Pharmacology at the University of Illinois and was finalized after his move to the Department of Pharmacology at Rush University Medical Center.

REFERENCES

1. Simionescu, M., Gafencu, A., and Antohe, F. (2002) *Microsc. Res. Tech.* **57,** 269–288
2. Mehta, D., and Malik, A. B. (2006) *Physiol. Rev.* **86,** 279–367
3. Predescu, S. A., Predescu, D. N., Knezevic, I., Klein, I. K., and Malik, A. B. (2007) *J. Biol. Chem.* **282,** 17166–17178
4. Michel, C. C., and Curry, F. E. (1999) *Physiol. Rev.* **79,** 703–761
5. Majno, G., and Palade, G. E. (1961) *J. Biophys. Biochem. Cytol.* **11,** 571–605
6. Robert, E. G., and Hunt, J. D. (2001) *Curr. Pharm. Des.* **7,** 1615–1626
7. Stafforini, D. M., McIntyre, T. M., Zimmerman, G. A., and Prescott, S. M. (2003) *Crit. Rev. Clin. Lab. Sci.* **40,** 643–672
8. Dvorak, H. F., Brown, L. F., Detmar, M., and Dvorak, A. M. (1995) *Am. J. Pathol.* **146,** 1029–1039
9. Roberts, W. G., and Palade, G. E. (1995) *J. Cell Sci.* **108,** 2369–2379
10. Garcia, J. G., Davis, H. W., and Patterson, C. E. (1995) *J. Cell Physiol.* **163,** 510–522
11. Lee, T. Y., and Gotlieb, A. I. (2003) *Microsc. Res. Tech.* **60,** 115–127
12. Adamson, R. H., Zeng, M., Adamson, G. N., Lenz, J. F., and Curry, F. E. (2003) *Am. J. Physiol.* **285,** H406–H417
13. Baldwin, A. L., and Thurston, G. (1995) *Am. J. Physiol.* **269,** H1528–H1537
14. Baldwin, A. L., and Thurston, G. (2001) *Crit. Rev. Biomed. Eng.* **29,** 247–278
15. Aktories, K., Barmann, M., Ohishi, I., Tsuyama, S., Jakobs, K. H., and Habermann, E. (1986) *Nature* **322,** 390–392
16. Aktories, K., and Barth, H. (2004) *Anaerobe* **10,** 101–105
17. Drenckhahn, D., and Ness, W. (1997) *The Endothelial Contractile Cytoskeleton*, Schauttauer, Stuttgard, Germany
18. Gottlieb, A. I., Langille, B. L., Wong, M. K., and Kim, D. W. (1991) *Lab. Invest.* **65,** 123–137
19. Pellegrin, S., and Mellor, H. (2007) *J. Cell Sci.* **120,** 3491–3499
20. Madara, J. L., Moore, R., and Carlson, S. (1987) *Am. J. Physiol.* **253,** C854–C861
21. Svensjo, E., and Grega, G. J. (1986) *Fed. Proc.* **5,** 89–95
22. Vandekerckhove, J., Schering, B., Barmann, M., and Aktories, K. (1988)

J. Biol. Chem. **263,** 696–700
23. Wegner, A., and Aktories, K. (1988) *J. Biol. Chem.* **263,** 13739–13742
24. Dejana, E. (1996) *J. Clin. Invest.* **98,** 1949–1953
25. Cohen, A. W., Carbajal, J. M., and Schaeffer, R. C., Jr. (1999) *Am. J. Physiol.* **277,** H2038–H2049
26. Rousseau, S., Houle, F., and Huot, J. (2000) *Trends Cardiovasc. Med.* **10,** 321–327
27. Snyder, F. (1995) *Biochem. J.* **305,** 689–705
28. Chignard, M., Le Couedic, J. P., Tence, M., Vargaftig, B. B., and Benveniste, J. (1979) *Nature* **279,** 799–800
29. Benveniste, J. (1989) *Adv. Prostaglandin Thromboxane Leukot. Res.* **19,** 355–358
30. Camussi, G., Bussolino, F., Tetta, C., Piacibello, W., and Aglietta, M. (1983) *Int. Arch. Allergy Appl. Immunol.* **70,** 245–251
31. Camussi, G., Aglietta, M., Malavasi, F., Tetta, C., Piacibello, W., Sanavio, F., and Bussolino, F. (1983) *J. Immunol.* **131,** 2397–2403
32. Axelrad, T. W., Deo, D. D., Ottino, P., Van Kirk, J., Bazan, N. G., Bazan, H. E., and Hunt, J. D. (2004) *FASEB J.* **18,** 568–570
33. Humphrey, D. M., McManus, L. M., Hanahan, D. J., and Pinckard, R. N. (1984) *Lab. Invest.* **50,** 16–25
34. Predescu, D., Ihida, K., Predescu, S., and Palade, G. E. (1996) *Eur. J. Cell Biol.* **69,** 86–98
35. Marrache, A. M., Gobeil, F., Jr., Bernier, S. G., Stankova, J., Rola-Pleszczynski, M., Choufani, S., Bkaily, G., Bourdeau, A., Srois, M. G., Vazquez-Tello, A., Fan, L., Joyal, J. S., Filep, J. G., Varma, D. R., Rbeiro-Da-Silva, A., and Chemtob, S. (2002) *J. Immunol.* **169,** 474–481
36. Bussolino, F., Silvagno, F., Garbarino, G., Costamagna, C., Sanavio, F., Arese, M., Soldi, R., Aglietta, M., Pescarmona, G., and Camussi, G. (1994) *J. Biol. Chem.* **269,** 2877–2886
37. Bussolino, F., Camussi, G., Aglietta, M., Braquet, P., Bosia, A., Pescarmona, G., Sanavio, F., D'Urso, N., and Marchisio, P. C. (1987) *J. Immunol.* **139,** 2439–2446
38. Halonen, M., Palmer, J. D., Lohman, I. C., McManus, L. M., and Pinckard, R. N. (1980) *Am. Rev. Respir. Dis.* **122,** 915–924
39. Garrett, T. A., Van Buul, J. D., and Burridge, K. (2007) *Exp. Cell Res.* **313,** 3285–3297
40. Smith, P. K., Krohn, R. I., Hermanson, G. T., Mallia, A. K., Gartner, F. H., Provenzano, M. D., Fujimoto, E. K., Goeke, N. M., Olson, B. J., and Klenk, D. C. (1985) *Anal. Biochem.* **150,** 76–85
41. Predescu, S., Predescu, D., and Palade, G. (2001) *Mol. Biol. Cell* **12,** 1019–1033
42. Patterson, R. L., van Rossum, D. B., and Gill, D. L. (1999) *Cell* **98,** 487–499
43. Surks, H. K., Riddick, N., and Ohtani, K. (2005) *J. Biol. Chem.* **280,** 42543–42551
44. Towbin, H., Staehelin, T., and Gordon, J. (1979) *Proc. Natl. Acad. Sci. U. S. A.* **76,** 4350–4354
45. Weiner, O. D., Servant, G., Welch, M. D., Mitchison, T. J., Sedat, J. W., and Bourne, H. R. (1999) *Nat. Cell Biol.* **1,** 75–81
46. Taylor, S. J., and Shalloway, D. (1996) *Curr. Biol.* **6,** 1621–16277
47. Cook, J. A., Albacker, L., August, A., and Henderson, A. J. (2003) *J. Biol. Chem.* **278,** 35812–35818
48. Garcia-Mata, R., Wennerberg, K., Arthur, W. T., Noren, N. K., Ellerbroek, S. M., and Burridge, K. (2006) *Methods Enzymol.* **406,** 425–437
49. Porter, K., Kelly, D., and Andrews, P. (1972) *Proceedings of the Fifth Annual Stereoscan Scanning Electron Microscope Colloquium, Morton Grove, IL, April*, p. 1244, Kent Cambridge Scientific Inc.
50. Braquet, P., Esanu, A., Buisine, E., Hosford, D., Broquet, C., and Koltai, M. (1991) *Med. Res. Rev.* **11,** 295–355
51. Qian, Y., Baisden, J. M., Westin, E. H., Guappone, A. C., Koay, T. C., and Flynn, D. C. (1998) *Oncogene* **16,** 2185–2195
52. Baisden, J. M., Gatesman, A. S., Cherezova, L., Jiang, B. H., and Flynn, D. C. (2001) *Oncogene* **20,** 6607–6616
53. Cicchetti, G., Allen, P. G., and Glogauer, M. (2002) *Crit. Rev. Oral Biol. Med.* **13,** 220–228
54. Walsh, C. T., Radeff-Huang, J., Matteo, R., Hsiao, A., Subramaniam, S., Stupack, D., and Heller Brown, J. (2008) *FASEB J.*, in press
55. Ryu, Y., Takuwa, N., Sugimoto, N., Sakurada, S., Usui, S., Okamoto, H., Matsui, O., and Takuwa, Y. (2002) *Circ. Res.* **90,** 325–332
56. Lum, H., and Malik, A. B. (1996) *Can. J. Physiol. Pharmacol.* **74,** 787–800
57. Verin, A. D., Patterson, C. E., Day, M. A., and Garcia, J. G. (1995) *Am. J. Physiol.* **269,** L99–L108
58. Bogatcheva, N. V., Garcia, J. G., and Verin, A. D. (2002) *Biochemistry (Mosc.)* **67,** 75–84
59. Lu, Z., and Wolf, M. B. (1993) *Circ. Shock* **41,** 8–18
60. Pinckard, R. N., McManus, L. M., Demopoulos, C. A., Halonen, M., Clark, P. O., Shaw, J. O., Kniker, W. T., and Hanahan, D. J. (1980) *J. Reticuloendothel. Soc.* **28,** 95s–103s
61. Pirotzky, E., Page, C. P., Roubin, R., Pfister, A., Paul, W., Bonnet, J., and Benveniste, J. (1984) *Microcirc. Endothelium Lymphatics* **1,** 107–122
62. Bjork, J., and Smedegard, G. (1983) *Eur. J. Pharmacol.* **96,** 87–94
63. Burhop, K. E., van der Zee, H., Bizios, R., Kaplan, J. E., and Malik, A. B. (1986) *Am. Rev. Respir. Dis.* **134,** 548–554
64. Nicholson-Dykstra, S., Higgs, H. N., and Harris, E. S. (2005) *Curr. Biol.* **15,** R346–R357
65. Svitkina, T. M., Bulanova, E. A., Chaga, O. Y., Vignjevic, D. M., Kojima, S., Vasiliev, J. M., and Borisy, G. G. (2003) *J. Cell Biol.* **160,** 409–421
66. Schirenbeck, A., Bretschneider, T., Arasada, R., Schleicher, M., and Faix, J. (2005) *Nat. Cell Biol.* **7,** 619–625
67. Meng, W., Numazaki, M., Takeuchi, K., Uchibori, Y., Ando-Akatsuka, Y., Tominaga, M., and Tominaga, T. (2004) *EMBO J.* **23,** 760–771
68. Fanning, A. S. (2001) in *Tight Junctions* (Cereijido, M., and Anderson, J., eds) pp 265–284, CRC Press, Inc. Boca Raton, FL
69. Ridley, A. J. (1999) *Prog. Mol. Subcell. Biol.* **22,** 1–22
70. Ridley, A. J., Allen, W. E., Peppelenbosch, M., and Jones, G. E. (1999) *Biochem. Soc. Symp.* **65,** 111–123
71. Adamson, R. H., Curry, F. E., Adamson, G., Liu, B., Jiang, Y., Aktories, K., Barth, H., Daigeler, A., Golenhofen, N., Ness, W., and Drenckhahn, D. (2002) *J. Physiol. (Lond.)* **539,** 295–308
72. Deo, D. D., Bazan, N. G., and Hunt, J. D. (2004) *J. Biol. Chem.* **279,** 3497–3508
73. Rhee, S. G. (2001) *Annu. Rev. Biochem.* **70,** 281–312
74. Fleming, I. N., Batty, I. H., Prescott, A. R., Gray, A., Kular, G. S., Stewart, H., and Downes, C. P. (2004) *Biochem. J.* **382,** 857–865
75. Fleming, I. N., Elliott, C. M., and Exton, J. H. (1998) *FEBS Lett.* **429,** 229–233
76. Waschke, J., Baumgartner, W., Adamson, R. H., Zeng, M., Aktories, K., Barth, H., Wilde, C., Curry, F. E., and Drenckhahn, D. (2004) *Am. J. Physiol.* **286,** H394–H401
77. Michiels, F., Stam, J. C., Hordijk, P. L., van der Kammen, R. A., Ruuls-Van Stalle, L., Feltkamp, C. A., and Collard, J. G. (1997) *J. Cell Biol.* **137,** 387–398